OBSERVATIONS OF BREAKUP PROCESSES OF LIQUID JETS USING REAL-TIME X-RAY RADIOGRAPHY*

N89-11160

J. M. Char,† K. K. Kuo,ζ and K. C. Hsieh‡
Department of Mechanical Engineering
The Pennsylvania State University
University Park, Pennsylvania 16802

Abstract

Liquid jet breakup mechanisms and processes have been studied extensively over the last one hundred years. However, since the region near the jet injector is too dense and optically opaque, conventional visualization cannot be applied with satisfactory experimental results. To unravel the liquid jet breakup process in the non-dilute region, a newly developed system of real-time X-ray radiography together with an advanced digital image processor and a high-speed video camera was used in this study. Based upon recorded X-ray images, the inner structure of a liquid jet during breakup was observed. The jet divergent angle, jet breakup length, and void fraction distributions along the axial and transverse directions of liquid jets, etc., were determined in the near-injector region. Both wall- and free-jet tests were conducted to study the effect of wall friction on the jet breakup process.

Introduction

Understanding the breakup mechanism of liquid jets in diesel engines, regenerative liquid propellant guns, and many other combustion and propulsion systems is extremely important, since the jet breakup process can strongly affect the jet divergent angle, the distributions of droplet size and velocity, and the mixing and combustion processes. As indicated in a detailed review paper by Arcoumanis and Whitelow,[1] numerous theoretical and experimental attempts have been made to study the stability and breakup phenomena of liquid jets ejected from nozzles. In recent years, Wu, Reitz and Bracco,[2] Birk and Reeves,[3] and Baev et al.[4] conducted intensive studies in the experimental investigation of breakup behavior in the near-injector region. Shimizu et al.[5] studied the breakup length of a high-speed jet by measuring the electrical resistance between a nozzle and a fine wire detector located in a spray jet. They found that breakup length decreases with increase in injection velocity, finally reaching a constant value.

In the theoretical analyses, the growth of initial perturbations on the liquid surface, the effects of liquid inertia, surface tension, viscous and aerodynamic forces on the jet were considered. The earliest development of a predictive model for the jet breakup was initiated by Rayleigh.[6,7] His linear stability analysis of an inviscid cylindrical liquid jet showed that an axisymmetric disturbance could be stable or unstable, depending upon the magnitude of the wavelength (stable for wavelengths less than the circumference of the jet, and unstable for other cases). Further investigations using linear stability analysis were conducted by Tyler and Richardson,[8] Schweitzer,[9] Merrington,[10] Levich[11], Dombrowski and Hooper,[12] and others. Based on these studies, the jet divergent angle near the injector exit, and jet breakup length and mean drop size near the lateral surface of the jet can be estimated from the Reynolds number, the Weber number, the density ratio of liquid to gas, and several empirical constants. The effect of viscosity was studied by Weber.[13] More recently, the effect of nonlinearity[14-19] has been considered and solved numerically in order to simulate more closely the jet breakup processes.

In the experimental studies, the core of the jet is optically opaque due to the high-density condition in the near-injector region. Hence, observations and measurements of the near-injector region are almost impossible. Consequently, most previous studies focused on the dilute region or on the jet boundary near the injector exit.[2] Due to the lack of quantitative test results in the near-injector region, the theoretical models developed for prediction of jet-core breakup length, mean drop size distribution, etc., have not yet been validated. The estimated jet profiles and characteristics at a given near-injector station were used as initial and/or boundary conditions in order to simulate the atomization and combustion processes in the dilute region; this, in turn, could cause errors and uncertainties in the theoretical predictions of combustion processes.

The purpose of the present study is to achieve a better understanding of the jet breakup process, using a newly developed system of real-time X-ray radiography together with an advanced digital image processor and a high-speed video camera. The specific objectives are: (1) to illustrate the differences between X-ray radiography images and regular high-speed movie films; (2) to measure jet velocity, jet breakup length, and void fraction distributions in the near-injector region; (3) to observe the evolution of the jet breakup and the formation of ligaments and droplets in the near-injector region in order to determine the inner structure of the liquid jets; and (4) to demonstrate the feasibility and advantage of using X-ray radiography in the jet breakup study. In order to study the effect of wall friction on the jet breakup process, both wall- and free-jet tests were conducted.

Experiment Apparatus

In the experimental approach, a test rig has been designed and fabricated to simulate both wall and free jets ejected from a two-dimensional slit with an aspect ratio of 10. The advantage of using a planar two-dimensional jet is to avoid the curvature effect which is inherently associated with circular or annular jets.[3] The side view of

*The authors are grateful to Professor V. Yang of PSU for his initial effort in this study. The assistance in test rig design by Dr. L. K. Chang and chamber fabrication by Mr. W. Loesch are also greatly appreciated.

†Ph.D. Candidate

ζDistinguished Alumni Professor of Mechanical Engineering, Associate Fellow of AIAA

‡Research Assistant, presently working at Sverdrup Technology, Inc., Cleveland, Ohio

the jet breakup process is much clearer in the planar two-dimensional case than in other cases. The schematic diagram of the test rig is shown in Fig. 1. A photograph of the test setup is shown in Fig. 2. In Fig. 1, the gap of the two-dimensional slit between elements 5 and 7 is 2 mm, and element 5 is an interchangeable piece for providing different lengths of the wall jet. When a piece of element 5 ends at the same location as element 7, the configuration is that of a free jet test case. A pressure transmitting rod is shown as element 4. Prior to the test, this rod was lifted by a vacuum pump. The liquid was then loaded through element 6 into the free volume beneath the rod and the entire slit region. The liquids used in tests were either water or Pantopaque ($C_{19}H_{29}IO_2$), a fluid used in medical X-ray examinations. The physical properties of the two test fluids are presented in Table 1. During the test, a solenoid valve was activated to introduce high-pressure nitrogen gas into the top portion of the test rig (see Fig. 2), thus pushing the rod downward to inject the liquid into the unconfined ambient air. A major portion of the Pantopaque was recovered for further use.

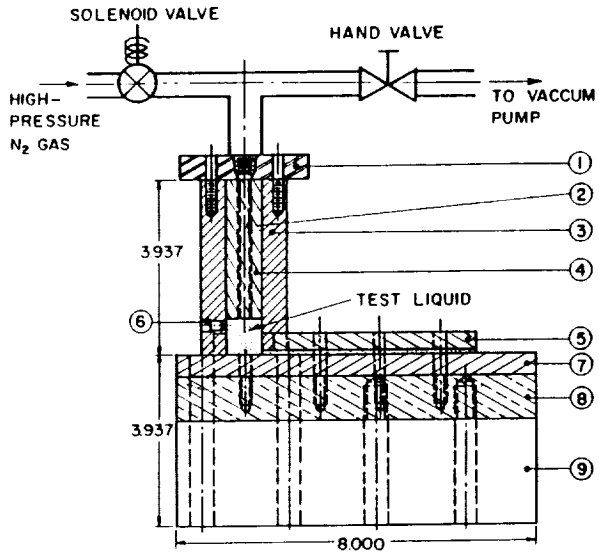

Fig. 1 Schematic Diagram of Test Rig Assembly for Two-Dimensional Wall or Free Jet Breakup Studies (1. top cover, 2. bolts, 3. liquid reservoir, 4. push rod, 5. top plate of slit, 6. liquid feeding hole, 7. base plate of slit, 8 and 9. test rig holder)

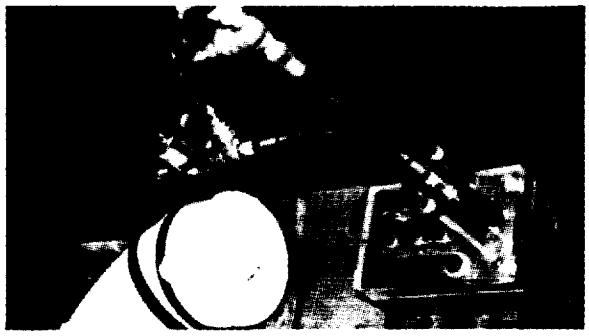

Fig. 2 Photograph of the Test Setup

Data Acquisition System

During the test, the instantaneous liquid jet contour was filmed by real-time X-ray radiography. Figure 3 shows the layout of various components of the radiography system. A continuous X-ray was generated from the Phillips MG 321 constant potential X-ray system. Two X-ray tubes [one with a focal spot combination of 0.2 x 0.2 mm/3.0 x 3.0 mm (MCN 167/160 kV), the other with a focal spot combination of 1.2 x 1.2 mm/4.0 x 4.0 mm (MCN 321/320 kV)] were employed to achieve different penetration depths and spatial resolution requirements. A lead diaphragm was installed at the exit port of the X-ray tube head to limit the angle of divergence of the X-ray beam and to confine the beam to the measuring section of the liquid jet test rig. (This also reduced unnecessary radiation exposure.) A second lead diaphragm with a larger opening was placed in front of the image intensifier to reduce scattered X-ray radiation and decrease the noise level on the fluorescent screen.

After passing through the test rig and liquid jet, X-ray signals were transformed to fluorescent light signals on the output screen of a tri-field image intensifier (Precise Optics, Model P1 2400 ATF, 4", 6", or 9" field diameter). The input fluor of the image intensifier was made of cesium iodide with a decay-time constant of 650 ns, and the output fluor was a p20 type with a 85 ns decay-time constant. These time constants are short enough to allow the motion analysis system to operate at its maximum framing rate without generating image blur.

The fluorescent light signal output from the image intensifier was recorded by a Spin Physics 2000 Motion Analysis System. This system can record up to 2000 fully digitized frames per second, or up to 12,000 digitized pictures per second with adjustable playback speed. The motion analysis system consists of the following subsystems:

a) a Spin Physics 2000 video camera with solid-state image sensor. The picture information goes to the console from the camera, and is processed into a frequency-modulated carrier that is recorded on tape.

b) a main electronic bin, which contains record and playback electronics, along with video output circuitry.

c) a tape transport, which drives the half-inch tape cassette at a maximum speed of 250 inches per second.

Digitized data was stored on a high-intensity magnetic recording tape and transferred to the digital image-processing system frame by frame for analysis through an IEEE-488 interface. The digital image-processing system consists of several major components:

a) a Quantex (QX-9210) digital image processor with two pipeline point processors, each with a random access image memory of 480 x 640 x 12 bits. The processors perform real-time image enhancements, including noise reduction, image subtraction, arbitrary contrast control, roam, and zoom. The processor can also be used to conduct such high-speed image analyses as brightness histogram, local contrast stretch, area and point brightness

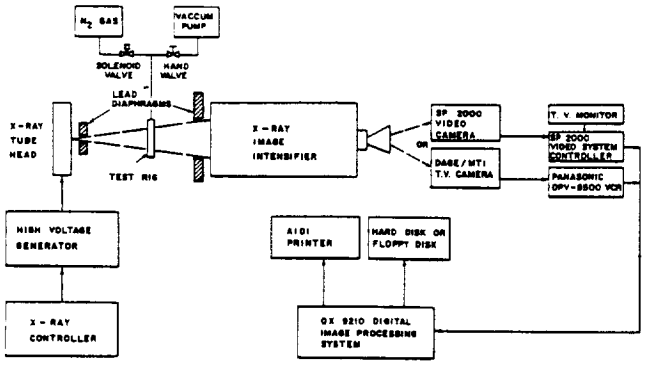

Fig. 3 Real Time X-ray Radiography and Digital Image Processing System

measurements, calibrated length and area measurements, Sobel edge enhancement, and so forth.

b) a mass storage device consisting of both a 2.4 MB dual 8" floppy diskette drive and a 50 MB hard disk for storage of image data.

c) a high-resolution videograph printer (AIDI CT1500) for producing large high-quality pictures on hard copies with 1660 lines/inch resolution.

Data Reduction Procedure

Besides observing the jet structure directly from the recorded film (both regular movie and X-ray films), more detailed and accurate data could be deduced by analyzing the X-ray intensity distribution across the jet in horizontal and vertical directions. Basically, an ideal radiography image of the liquid jet can be determined from the assumptions that 1) X-ray radiation is generated from a point source via an infinitely small focal spot, 2) X-ray is only attenuated by photoelectric absorption, and 3) distribution of X-ray intensity over the input screen of an image intensifier is uniform. As shown in Fig. 4, the X-ray intensity distribution on a y = constant plane can be evaluated by the following equation:

$$I(x) = I_o \, EXP \, [-mW(x)] \qquad (1)$$

where m is the linear attenuation coefficient of photoelectric absorption, and W(x) is the local sum of the intercepted width of the liquid in the two-phase jet. Due to the X-ray beam attenuation across the liquid jet, the following test data can be obtained using the digital image-processing system:

a) Measurement of Radiance or Pixel Value: The radiance (or pixel value) of any arbitrary point of interest in the jet can be obtained by moving the cursor to that point. The local radiance and the x, y coordinates of the location can be displayed on the screen.

b) Measurement of Area and Pixel Value: The software program combines a measurement of an area with a measurement of the integrated pixel values (or total radiance) within the area. The calculated average pixel value within the area is also displayed on the screen. This feature can be used to detect the local void fraction level

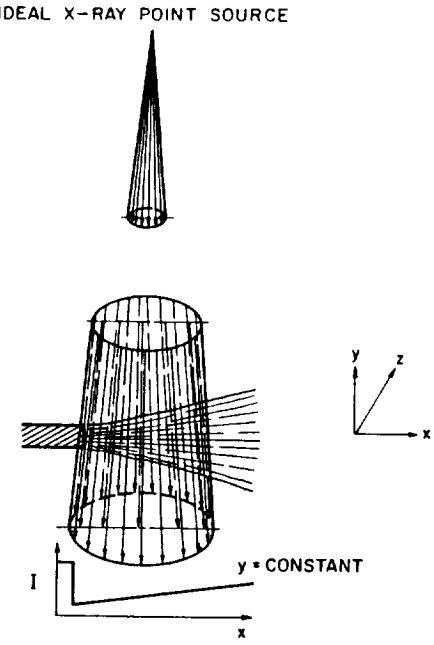

Fig. 4 X-ray Intensity Distribution Across a Liquid Jet Under Idealized Conditions

from the X-ray radiograph for a specified jet region (see Fig. 5).

c) Profile Analysis: Figures 6 and 7 show the measurement of the pixel value of two scan lines--one parallel and one perpendicular to the jet core and head regions. Both end at the cursor point. From these profiles, the void-fraction distribution can be deduced for a certain cross-section of the jet.

d) Histogram Analysis: This procedure consists of measuring the frequency of occurrence of pixel values within a selected boundary of a rectangle. Such distributions can be used to detect jet breakup phenomena in the core region. Keeping the axial length of rectangular area constant by varying the width of the rectangle, different sets of histograms can be obtained. These are arranged into a series of histograms (see Fig. 8).

e) Isophote Analysis: Using the data reduction program, certain regions of the viewing area with the same range of pixel values can be replaced by white spots. This feature makes it possible to observe the contours of different radiances. The inner structure of a liquid jet can, therefore, be studied by selecting different pixel values (see Fig. 13, to be discussed later in the results section).

Finally, jet-head velocities in both axial and radial directions can be deduced from the recorded film by using the elapsed time and displacement of reticle lines on the monitor of the Spin Physics Camera System.

Discussion of Results

A series of high-speed motion pictures

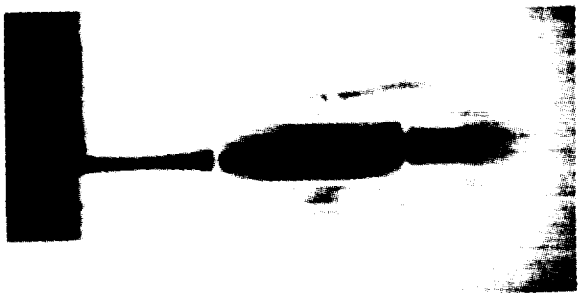

Fig. 5 Measurement of Area and Pixel Value of a Liquid Jet

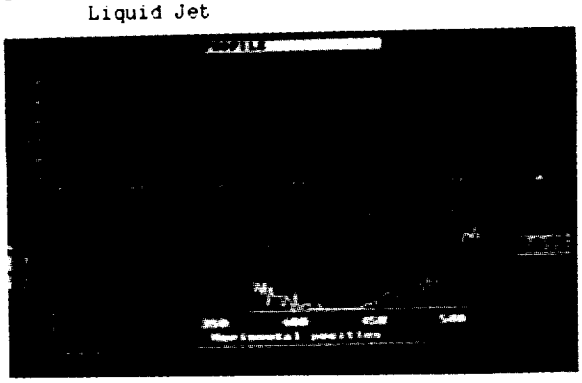

Fig. 6 Horizontal X-ray Intensity Profile at the Center Plane of a Liquid Jet

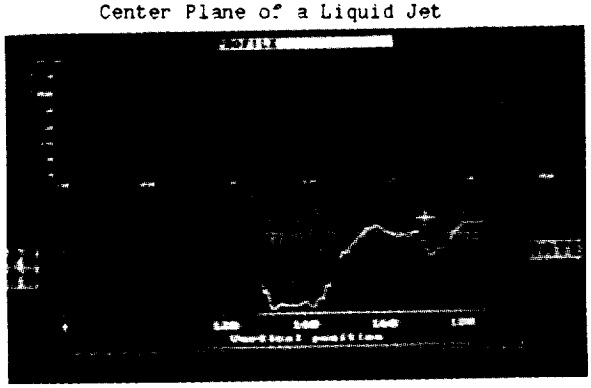

Fig. 7 Vertical X-ray Intensity Profile at a Distance from Jet Exit

showing the breakup process of a plane wall jet is given in Fig. 9. Several interesting phenomena of wall jet evolution and breakup can be noted from these photographs. In Fig. 9a, as the liquid jet traveled along the wall surface in the early stage, the head region diverged in the upward direction. A thin sheet of liquid was formed ahead of the main jet, as shown in Fig. 9b. This thin sheet of liquid surface is believed to be caused by shedding phenomena introduced by the inertia of the fast-moving liquid near the free surface of the engulfing wave front. Near the top surface, the velocity of the liquid is much higher than that near the wall, since the viscous force is much smaller at the free surface. As time progressed, this sheet became more evident, and the head region expanded further (see Fig. 9c). In Fig. 9d, the main jet accelerated and merged with part of the thin liquid sheet. In the later stage, the so-called Klystron effect[20] was visible. This effect was introduced by the acceleration of the main jet, which had higher axial momentum to catch up with the precursor jet mass. Due to the coalescence of the fast and slow moving fluids, the width of the jet spread in transverse directions. This spreading also made the jet-head portion more symmetric. In the meantime, several ligaments and numerous droplets were formed as the head region expanded further. Such a breakup process greatly influenced vaporization, ignition, and combustion of liquid sprays.

A set of high-speed photographs for the free jet case is shown in Fig. 10. The jet head was quite symmetric as it expanded in the transverse direction. The shape of the jet head changed from a round cross section to a mushroom-shaped contour. The Klystron effect can also be seen in Figs. 10d, e, and f. The jet head in Fig. 10e became spear shaped with a sharp leading edge. Some ligaments and droplets were formed (see Fig. 10f) near the boundary of the liquid-gas interface.

To demonstrate the differences between conventional high-speed movie film and high-speed X-ray radiography, a set of X-ray movie films showing free jet breakup processes is given in Fig. 11. It is quite obvious that, unlike the conventional high-speed movie film, the radiance of the jet head region is highly nonuniform. The

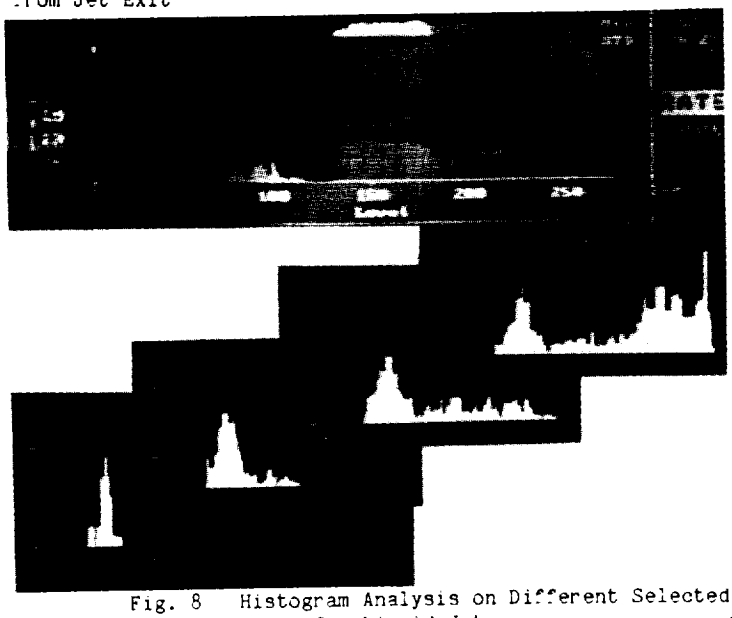

Fig. 8 Histogram Analysis on Different Selected Area of a Liquid Jet

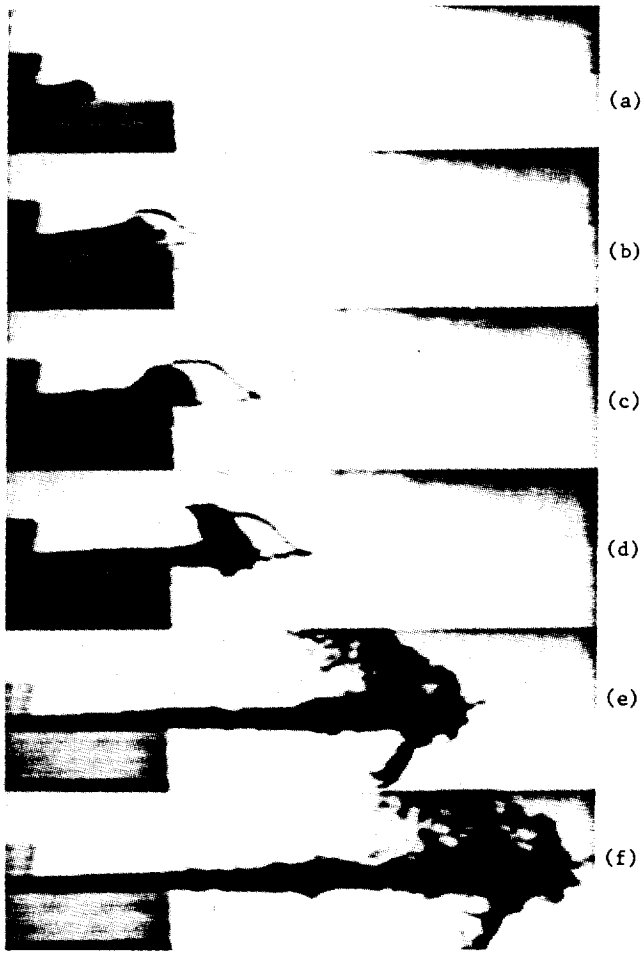

Fig. 9 Interesting Phenomena of a Plane Wall Liquid Jet Breakup Process (From High-Speed Movie Film)

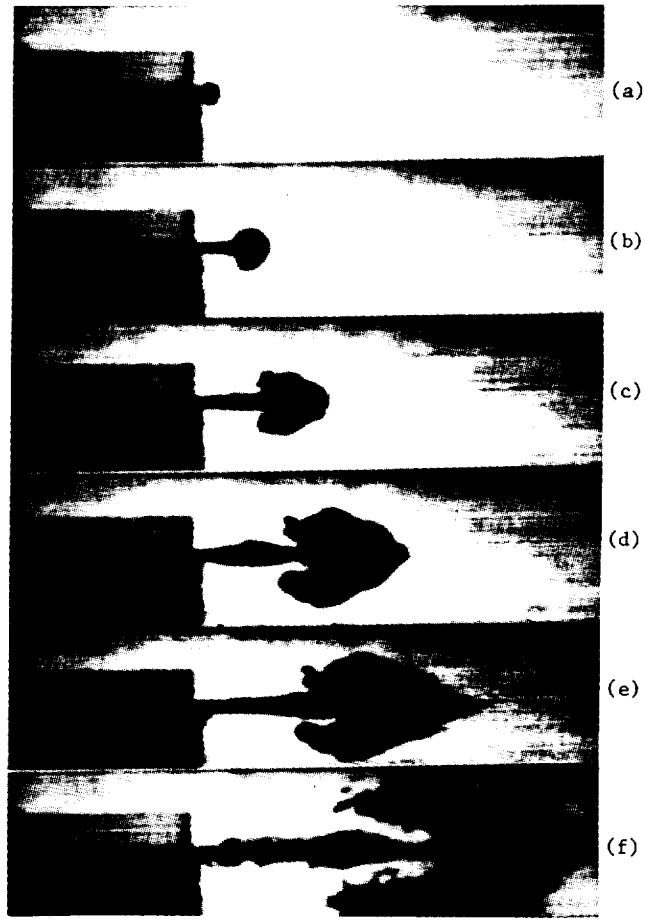

Fig. 10 Evolution of a Plane Free Liquid Jet Breakup (From High-Speed Movie Film)

inner structure of the jet can, therefore, be observed and analyzed from these images.

An enlarged photograph of the X-ray radiography, obtained from the zoom feature, is shown in Fig. 12. Figure 13 gives a set of pictures of the same object, but with different levels of radiance. The variation in contour of the isophote shows the detailed structure of the nondilute liquid jet. Although some pulsed X-ray photographs were obtained by Baev, et al.,[4] for liquid jet, the detailed inner structure of a non-dilute jet during the process of breakup has never been observed before, to the best of the authors' knowledge.

Using the Quantex Image Analyzer, the void fraction distribution in the vertical direction (normal to the jet axis) can be deduced for any axial location. Figure 14 shows the void fraction distribution across the widest jet head of photograph 12 (see also Fig. 7 cursor station). Near the centerplane (y = 0), the void fraction is much lower than that at the jet boundary [when y is approximately equal to 4H (gap width of the jet exit)]. The magnitude of the local void fraction is taken to be proportional to the local pixel value, (see Fig. 7) i.e.,

$$\phi(x,y) = 1 + 1/m(x,y) \ln I(x,y)/I_0 \qquad (2)$$

where I_G and I_L represent the intensity (pixel value) of pure gas and liquid, respectively. For Pantopaque in air, the values of I_G and I_L were 130 and 20, corresponding to the X-ray setting for most tests. It is useful to note that the distance between the X-ray tube head and the image intensifier was held constant during these tests.

A typical void fraction distribution for a wall jet is shown in Fig. 15. It is evident that near the wall (y/H = 0.5) the void fraction was almost zero, while the value of ϕ was quite close to unity near the outer edge of the wall jet.

A question about the effect of diffraction and scattering from multiple interfaces on the accuracy of Eq. (2) has been addressed. Equation (2) essentially assumes that diffraction and scattering from multiple interfaces have no effect on the reduction of void fraction from intensity measurements. To verify the weak dependence of intensity on the number and orientation of interfaces, two strands of rectangular-shaped solid propellant grains from the same batch with equal length were tested. One strand was cut into 10 sections with different angles to the main axis. The other strand remained as an integral piece. The two strands were placed on a platform adjacent to each other and viewed by X-ray from their end surfaces. The local intensity distribution for each strand was obtained and compared. It was found that the intensity of the uncut piece is only 5.80% higher than that of the chopped strand. This implies that the intensity of the X-ray radiography is minimally affected by the number and orientation of the interfaces. The loaded fraction (1-ϕ) deduced from Eq. (2) corresponds to

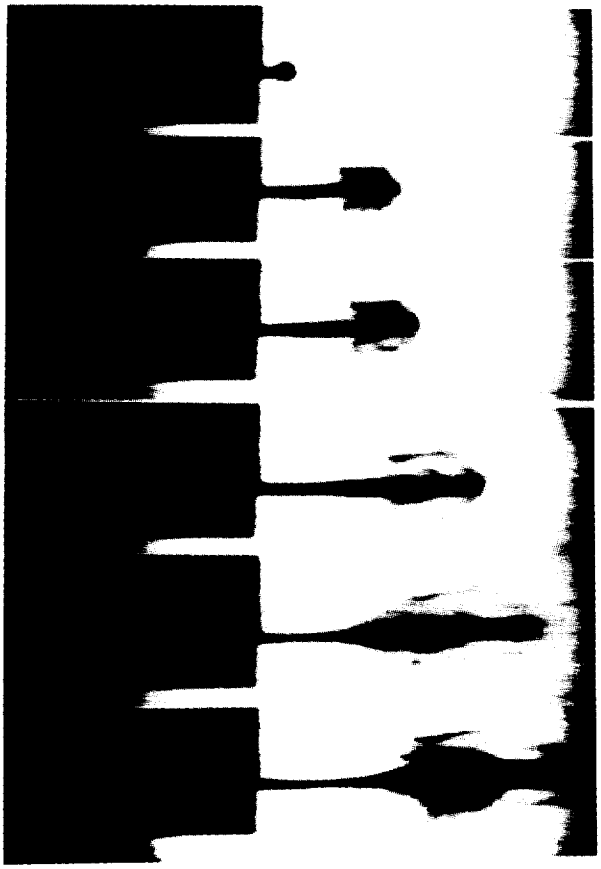

Fig. 11 Evolution of a Plane Free Liquid Jet Using the X-ray Radiography System

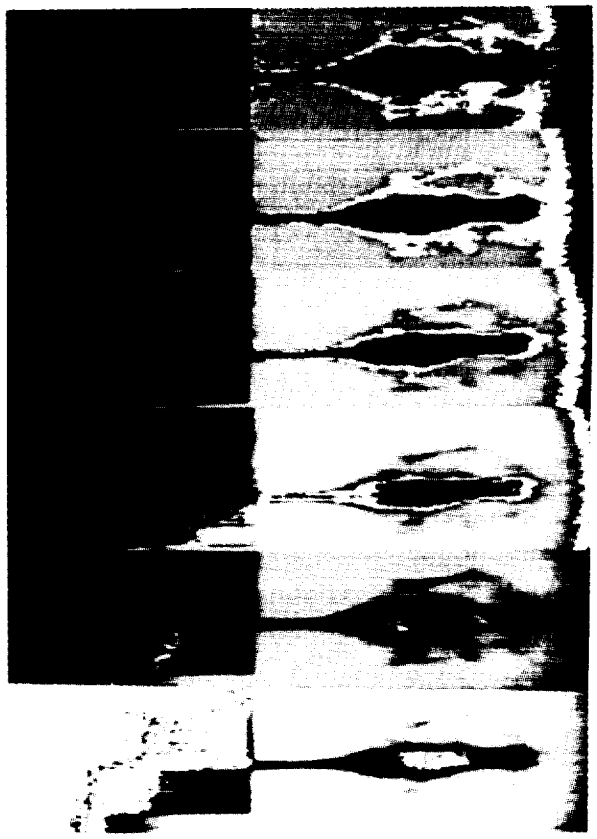

Fig. 13 Isophote Analysis Shows the Inner Structure of a Liquid Jet Using Different X-ray Intensity Levels

the total width of the liquid intercepted by the X-ray.

The jet spreading angle in the y direction is of interest in spray combustion. The angle θ can be determined from the instantaneous jet velocities in both x and y directions. The jet head velocities (u and v) in the x and y directions are deduced from the displacements of the vertical and horizontal lines on the Spin Physics monitor. The spread angle is defined as

$$\theta = 2 \tan^{-1} (v/u) \qquad (3)$$

A plot of half spread angle ($\theta/2$) versus jet head axial velocity (u) is shown in Fig. 16. For both wall- and free-jet experiments, spread angles decrease as jet head velocity increases. This is due to the fact that when a jet has higher axial momentum, the rate of spreading is lower. Based upon the data shown in Fig. 16, the wall jet spread out more than the free jet due to the momentum distribution effect in the wall jet. Near the wall surface, the non-slip condition must be satisfied, and hence the liquid near the free surface has a higher velocity than the free jet case for the same jet head velocity.

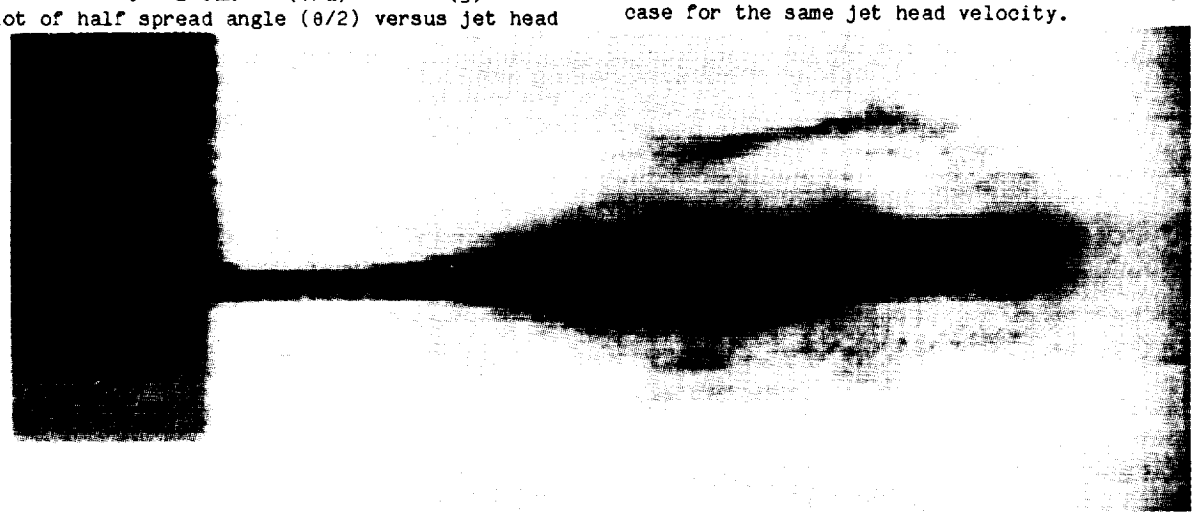

Fig. 12 Enlarged Picture of a Liquid Jet from X-ray Image

The jet surface breakup distance (L_{SB}) and the jet core breakup distance (L_{CB}) from the exit station are also important in spray combustion. Figure 17 plots these two distances versus jet head velocity. Determination of L_{SB} was based upon the location of the first discernible divergence of liquid from the jet surface. The value of L_{CB} was determined from the abrupt increase of intensity along the axial intensity distribution at the centerplane of the jet. For both wall and free jets, L_{SB} increased with jet head velocity due to the higher inertia of the liquid jet which delays the jet surface breakup. However, L_{CB} decreased while jet head velocity increased for both wall and free jets due to the fact that higher velocity jets may cause droplet collision and coalescence to occur earlier, generating an inhomogeneous axial intensity profile. It should be noticed that the jet core breakup distance used here is different from that used in previous studies. (In earlier studies, L_{CB} is the length beyond which the jet is no longer continuous.) At the same jet head velocity, wall jets have longer L_{SB} and L_{CB} than free jets due to the fact that wall jets, which are affected significantly by the stronger viscous force, retard the core breakup. In comparing surface breakup length, at the same value of jet head velocity, the wall jet has lower momentum than the free jet; hence, breakup length is longer.

Summary and Conclusions

1) The advantages of using real-time X-ray radiography for liquid-jet breakup measurements are summarized below:
   a) X-ray can partially penetrate through the liquid jets, even in the dense regions. Therefore, it is feasible to determine the instantaneous inner structure of the jet in the near-injector region during the jet breakup processes.
   b) X-ray radiography is a nonintrusive technique which does not affect the liquid jet breakup processes and is superior to other methods.
   c) The real-time feature of X-ray radiography gives the entire history of the jet breakup event instead of a few snapshots. The X-ray motion pictures taken during the test event can be played back immediately at a lower speed for detailed flow visualization and analysis.
   d) All data are in digital form and are convenient for recording, analysis, transfer, and storage in computers.
2) Based upon the recorded X-ray images analyzed on a digital image processor, jet divergent angle, jet breakup length, and jet void fraction distributions can even be measured in the near-injector region.
3) The effect of wall friction on the jet breakup process was observed by conducting wall- and free-jet tests. While the spread angle is larger for the same jet head velocity, longer distances are required for the surface and core to break up in the case of wall jet.
4) To understand the jet breakup mechanism, more detailed studies are required. Future tests should be conducted under varied conditions, such as different pressure and density levels in the gas phase, higher liquid-jet velocity ranges, various test liquids, different jet nozzle geometries, etc. The development of a comprehensive theoretical model for the near-injector region is also necessary. The predicted results should be compared with experimental data for model validation.

References

1. Arcoumanis, C. and Whitelaw, J. H., "Fluid Mechanics of Internal Combustion Engines: A Review," International Symposium on Flows in Internal Combustion Engines - III, Eds., T. Uzkan, W. G. Tiederman, J. M. Novak, ASME FED-Vol. 28, New York, 1985, pp. 1-17.
2. Wu, K.-J., Reitz, R. D. and F. V. Bracco, "Measurements of Drop Size at the Spray Edge Near the Nozzle in Atomizing Liquid Jets," Phys. Fluids, 29, 1986, pp. 914-951.
3. Birl, A. and Reeves, P., "Annular Liquid Propellant Jets - Injection, Atomization and Ignition," BRL Report, February, 1986.
4. Baev, V. K., Bazhaikin, A. N., Buzukov, A. A., and Timoshenko, B. P., "Experimental Study of the Development and Structure of High-Velocity Liquid Jets in Air," Progress in Astronautics and Aeronautics, Vol. 105, 1986, p. 104.
5. Shimizu, M., Arai, M. and Hiroyasu, H., "Measurements of Breakup Length in High-Speed Jets," Bull. of JSME, Vol. 27, No. 230, p. 1709, 1984.
6. Rayleigh, W. S., "On the Instability of Jets," Proc. London Math. Soc., V. X, 1879, p. 4.
7. Rayleigh, W. S., "On the Capillary Phenomena of Jets," Proc. Royal Soc., V. XXIX, 1879, p. 71.
8. Tyler, E. and Richardson, E. G., "The Characteristic Curves of Liquid Jets," Proc. Phys. Soc., V. 37, 1925, p. 297.
9. Schweitzer, P. H., "Mechanism of Disintegration of Liquid Jets," J. Appl. Physics, V. 8, 1937, p. 513.
10. Merrington, A. C. and Richardson, E. G., "The Breakup of Liquid Jets," Proc. Phys. Soc., V. 59, No. 331, 1947, p. 1.
11. Levich, V. G., Physiochemical Hydrodynamics, Prentice-Hall, New Jersey, 1962.
12. Dombrowski, N. and Hooper, P. C., "The Effect of Ambient Density on Drop Formation in Sprays," Chem. Eng. Sci., Vol. 17, 1962, pp. 291-305.
13. Weber, C., "Zum Zerfall eines Flussigkeitsstrables," ZAMM, V. 2, 1931, p. 136.

14. Chaudhary, K. C. and Redekopp, L. G., "The Nonlinear Capillary Instability of a Liquid Jet - Part 1 - Theory," J. Fluid Mech., V. 96, p. 2, 1980.

15. Chaudhary, K. C. and Maxworthy, T., "The Nonlinear Capillary Instability of a Liquid Jet - Part 2 - Experiments on Jet Behavior Before Droplet Formation," J. Fluid Mech., V. 96, 1980, p. 275.

16. Lafrance, P., "Nonlinear Breakup of a Liquid Jet," The Physics of Fluids, V. 17, No. 10, 1974, p. 1913.

17. Lee, H. C., "Drop Formation in a Liquid Jet," IBM J. Res. Develop., V. 18, 1974, p. 364.

18. Nayfeh, A. H., "Nonlinear Stability of a Liquid Jet," The Physics of Fluids, V. 13, No. 4, 1970, p. 841.

19. J. K. Dukowicz, "A Particle-Fluid Numerical Method for Liquid Sprays," J. Comp. Phys., Vol. 35, 1980, pp. 229-253.

20. Fenwick, J. R. and Bugler, G. J., "Oscillatory Flame Front Flow Rate Amplifications Through Propellant Injection Ballistics (The Klystron Effect). Third ICRPG Combustion Conference, CPIA Pub. No. 138, Vol. 1, February, 1967, p. 417.

TABLE 1. PHYSICAL PROPERTIES OF TEST LIQUIDS

Type	Viscosity (poise)	Density (gm/cm^3)	Surface Tension (dynes/cm)
Water	0.01	1.0	72.7
Pantopaque ($C_{19}H_{29}IO_2$)	0.051	1.259	32.1

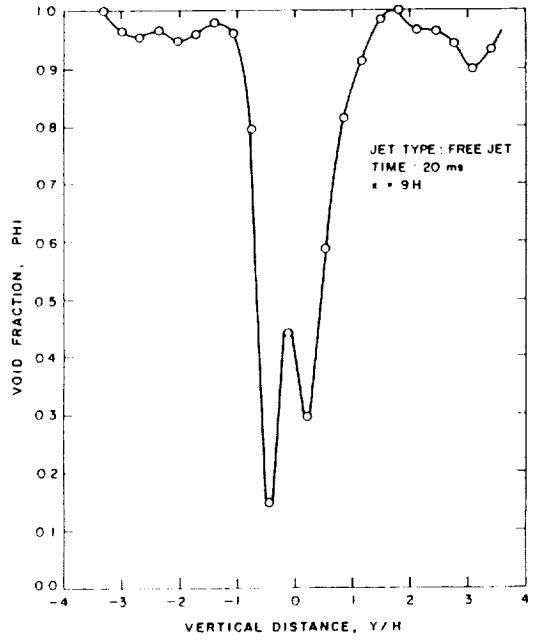

Fig. 14 Void Fraction Distribution Across the Widest Jet-Head Region (Plane Free Jet Case)

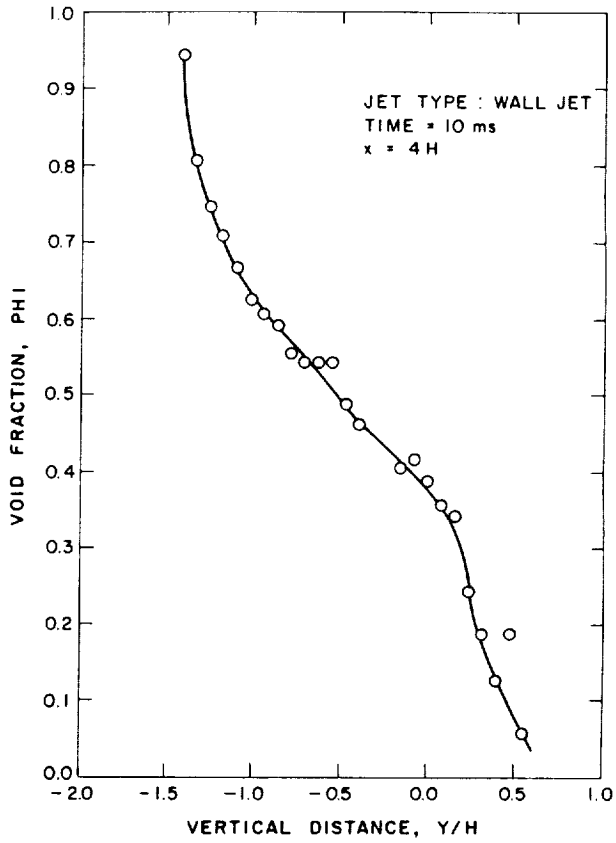

Fig. 15 Void Fraction Distribution Across the Widest Jet-Head Region (Plane Wall Jet Case)

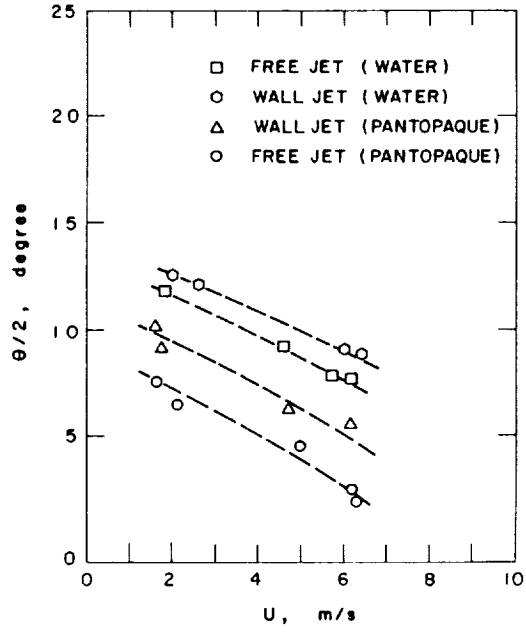

Fig. 16 Liquid Jet Divergent Angle Under Different Jet-Head Velocities

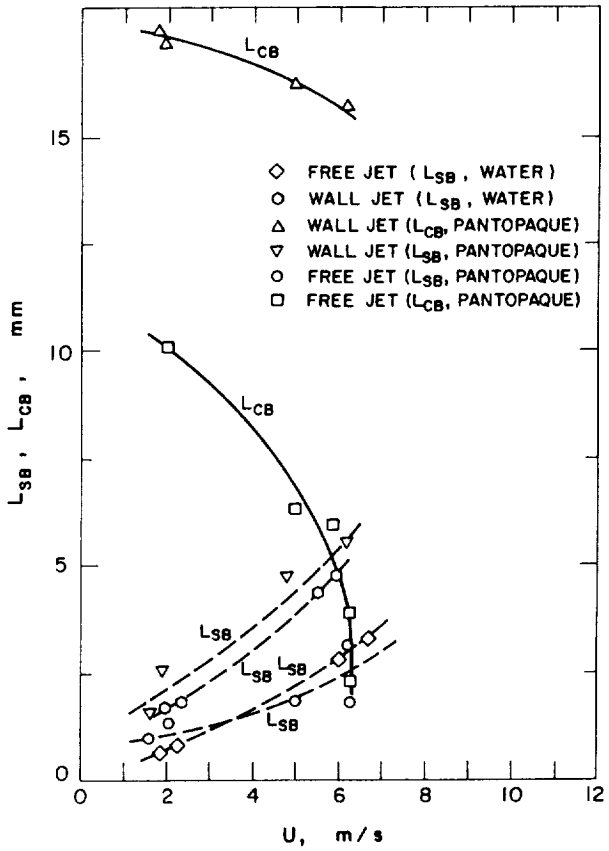

Fig. 17 Liquid Jet Breakup Length Under Different Jet-Head Velocities

Editor's Narrative:

Round-Table Discussion: Physical, Model, Numerical and Experimental Aspects of Mixing and Demixing Processes in Multiphase Flows

At the conclusion of the first day of presentations a discussion was opened in the general areas of physical, model, numerical and experimental aspects of mixing and demixing processes in multiphase flows. Two specific topics became the focus of the discussion. These were the relative merits of the continuum vs. Lagrangian-Eulerian frameworks for developing multiphase flow theories and the accuracy of the turbulence models used within these theories.

By the lack of discussion, it would appear that laminar flow about a single spherical particle, at small or zero Reynolds number, leading to expressions for the drag and migrations in idealized mechanical two-phase flows are not imperative issues. This is despite the fact that most theories of turbulent multiphase flow, whether continuum or Lagrangain-Eulerian in origin, accept aspects of Stokes flow analysis within the models for the phase coupling drag. Hence, the accurate description of the forces on a single particle in various circumstances is important for a wide variety of flows. In addition, there exists a prevailing attitude that the diffusion potentials due to the turbulence of the continuous fluid phase dominates any transverse or migrational motions of the dispersed phase. However, it should be noted that laminar processes resulting in transverse particle migrations may be of consequence within the viscous sublayer of turbulent flows if the particle sizes are small relative to the viscous sublayer thickness. This may be the case for such phenomenon as near wall particle depletion, as observed in turbulent multiphase pipe and channel flows. Lastly, within this same context, it should be noted that there are particle migration processes which may be analyzed by in-the-mean or laminar theory for some scale of 'large' or 'heavy' particles relative to the turbulence. For example, a baseball, by imparting a spin to it can be made to curve (migrate laterally) through the atmospheric boundary layer with apparent disregard for the random diffusion potentials placed on it by the turbulent air.

In the discussion of the relative merits of the continuum vs. the Lagrangian-Eulerian frameworks for developing theories of multiphase flows, one of the shortcomings of the continuum approach was immediately pointed out. Specifically, the continuum approach requires *a priori* acceptance of the assumption that the particles are of a single size category and have identical mechanical properties. Thus, if the particles or droplets are a variety of different sizes or vary in mechanical properties then the 'two-fluid' model has become the 'many-fluid' model. This results in losing one of the original benefits of the continuum theories for two-phase flow, that being computational efficiency. This raised the question as to whether or not the continuum theories are an artifact of the pre-supercomputer era. A conclusion on this question was not reached. In defense of the continuum approach to modeling two-phase flow it was pointed out that a well posed continuum theory does not contain the implicit geometric dependencies that a Lagrangian-Eulerian scheme contains. In addition, continuum theories have been used successfully to provide dispersed phase field variable information in situations where the added complexity of tracking individual particles was not warranted.

Due to the stochastic nature and high frequency of collision between particles or droplets, a consensus was reached that continuum models may provide a more tractable approach than Lagrangian-Eulerian schemes for modeling dense two-phase flows. However, advances within this area will require constitutive relationships for the dispersed phase spherical and deviatoric stress, separate from those of the continuous fluid phase. The development of these relationships will have many of the same problems faced in trying to derive viscosity and strain-displacement relationships from kinetic gas theory. Advantages of the intuitively satisfying Lagrangian-Eulerian approach to multiphase flow theory were discussed. The 'particle tracking' allows for the coupling of the fluid and particle at a level consistent with single particle hydrodynamic analysis. This approach, despite its requirement for increased computational resources can provide a very detailed level of information on field variables, including the spectrum of a stochastic variable at any point in the domain. Since it is usually the average behavior of any given variable, for example particle velocity, that is desired this stochastic response is averaged statistically over an ensemble of realizations. The result is to produce information at the same level as is available from continuum theory, that is, averaged fields. This highlights one of the primary differences between the continuum vs. the Lagrangian-Eulerian approach to multiphase flow modeling. Continuum theories give averaged field information from averaged conservation equations. On the other hand, Lagrangian-Eulerian theories will provide for the calculation of stochastic fields, from an ensemble of 'exact' conservation equations. Averaged information from Lagrangian-Eulerian theories requires the averaging of fields.

The modification or modulation of the turbulence structure of the continuous fluid phase due to the presence of the dispersed phase was discussed. Even at dilute concentrations, the coupling of the phases via drag will result in a modification of the production and dissipation of turbulent kinetic energy. Questions as to whether or not the presence of the dispersed phase will always enhance dissipation of fluid phase turbulent kinetic energy ensued and references to experimental observations were made. This led to the discussion of the models for the turbulent time scales of the dispersed phase and the continuous phase. A passive dispersed phase would have a relaxation time that approaches zero and it would follow the continuous phase turbulent and mean motions exactly. On the other hand, the relaxation time of the dispersed phase may be very large in which case the motion of the dispersed phase would be unaffected by the turbulence of the continuous phase. Unfortunately, in many turbulent multiphase flows of practical interest there exists a spectrum of dispersed phase time and length scales. Further complexity is introduced when it is pointed out that, despite the abundant use of single time and length scale models, single phase turbulent fluid flow is also dominated by a variety of length and time scales over the domain of the flow. Hence, the need for improved models of turbulence, for use in theories of single phase flow as well as multiphase flow was recognized. Concerning an earlier argument, it was pointed out that regardless of the level of physical detail or lack thereof of the continuum or the Lagrangian-Eulerian theory, they both suffer from inadequate turbulence models. Any advantage in accuracy gained from using one theoretical approach over the other may, in some cases, be washed-out by the inaccuracies inherent in the common turbulence model.

The wisdom and desirability of repeating this workshop at sometime in the future was noted in closing.